A rogues gallery of Andromeda's dwarf galaxies – II. Precise distances to 17 faint satellites

Daniel Weisz, Andrew Dolphin, Nicolas F. Martin, Saundra Albers, Michelle Collins, Annette Ferguson, Geraint Lewis, a Dougal Mackey, Alan Mcconnachie, R Michael Rich, et al.

Monthly Notices of the ROYAL ASTRONOMICAL SOCIETY

MNRAS **489,** 763–770 (2019) doi:10.1093/mnras/stz1984
Advance Access publication 2019 July 22

A rogues gallery of Andromeda's dwarf galaxies – II. Precise distances to 17 faint satellites

Daniel R. Weisz [1]★ Andrew E. Dolphin,[2] Nicolas F. Martin,[3,4] Saundra M. Albers [1] Michelle L. M. Collins [5] Annette M. N. Ferguson,[6] Geraint F. Lewis [7] A. Dougal Mackey,[8] Alan McConnachie,[9] R. Michael Rich [10] and Evan D. Skillman[11]★

[1]*Department of Astronomy, University of California, Berkeley, CA 94720, USA*
[2]*Raytheon, 1151 E. Hermans Road, Tucson, AZ 85756, USA*
[3]*Observatoire Astronomique de Strasbourg, Université de Strasbourg, CNRS, UMR 7550, F-67000 Strasbourg, France*
[4]*Max-Planck-Institut für Astronomie, Königstuhl 17, D-69117 Heidelberg, Germany*
[5]*Department of Physics, University of Surrey, Guildford GU2 7XH, Surrey, UK*
[6]*Institute for Astronomy, University of Edinburgh, Royal Observatory, Blackford Hill, Edinburgh EH9 3HJ, UK*
[7]*Sydney Institute for Astronomy, School of Physics, A28, The University of Sydney, NSW 2006, Australia*
[8]*Research School of Astronomy and Astrophysics, Australian National University, Canberra, ACT 2611, Australia*
[9]*National Research Council, Herzberg Institute of Astrophysics, 5071 West Saanich Road, Victoria, BC V9E 2E7, Canada*
[10]*Department of Physics and Astronomy, University of California, Los Angeles, PAB, 430 Portola Plaza, Los Angeles, CA 90095-1547, USA*
[11]*Minnesota Institute for Astrophysics, University of Minnesota, Minneapolis, MN 55441, USA*

Accepted 2019 July 12. Received 2019 July 12; in original form 2019 June 11

ABSTRACT

We present new horizontal branch (HB) distance measurements to 17 of the faintest known M31 satellites ($-6 \lesssim M_V \lesssim -13$) based on deep *Hubble Space Telescope* (*HST*) imaging. The colour–magnitude diagrams extend ∼1–2 mag below the HB, which provides for well-defined HBs, even for faint galaxies in which the tip of the red giant branch (TRGB) is sparsely populated. We determine distances across the sample to an average precision of 4 per cent (∼30 kpc at 800 kpc). We find that the majority of these galaxies are in good agreement, though slightly farther (0.1–0.2 mag) when compared to recent ground-based TRGB distances. Two galaxies (And IX and And XVII) have discrepant *HST* and ground-based distances by ∼0.3 mag (∼150 kpc), which may be due to contamination from Milky Way foreground stars and/or M31 halo stars in sparsely populated TRGB regions. We use the new distances to update the luminosities and structural parameters for these 17 M31 satellites. The new distances do not substantially change the spatial configuration of the M31 satellite system. We comment on future prospects for precise and accurate HB distances for faint galaxies in the Local Group and beyond.

Key words: galaxies: distances and redshifts – galaxies: dwarf – Local Group.

1 INTRODUCTION

The number of known Andromeda satellite dwarf galaxies has dramatically increased over the last decade, mainly due to two large photometric surveys of this region of the sky. The Sloan Digital Sky Survey (Abazajian et al. 2003) enabled the discovery of a handful of relatively bright ($M_V < -8.5$) systems from an inhomogeneous and shallow surveying of the M31 surroundings (e.g. Zucker et al. 2004, 2007; Slater, Bell & Martin 2011; Bell, Slater & Martin 2011). The Pan-Andromeda Archaeological Survey (PAndAS; McConnachie et al. 2018) filled the need for a survey dedicated to the study of the stellar populations within the halo of the Andromeda galaxy, out to projected distances of ∼150 kpc. PAndAS alone has enabled the discovery of 15 unambiguous new Andromeda dwarf spheroidal galaxies (e.g. Martin et al. 2006, 2009, 2013b; Ibata et al. 2007; McConnachie et al. 2008; Richardson et al. 2011) with luminosities ranging from $M_V \sim -6.0$ to -10.0 ($M_\star \sim 10^{4-6} M_\odot$). More recently, the Panoramic Survey Telescope and Rapid Response System (Pan-STARRS; Chambers et al. 2016) also uncovered a handful of new Andromeda dwarf galaxies at larger projected distances than the PAndAS discoveries (e.g. Martin et al. 2013a,c).

A main goal of these, and other, surveys have been to establish basic properties of M31 satellites (e.g. mass, size, distance, and chemical composition; McConnachie et al. 2005; McConnachie & Irwin 2006; Kalirai et al. 2010; Tollerud et al. 2012; Collins et al.

★ E-mail: dan.weisz@berkeley.edu (DRW); skillman@astro.umn.edu (ES)

2013; Vargas, Geha & Tollerud 2014; Ho et al. 2015; Martin et al. 2016; Martínez-Vázquez et al. 2017), all of which are necessary to provide further insight into the evolution of satellites within the M31 ecosystem.

Secure distances to each of the M31 satellites are essential to virtually all other science goals. There is a long history of M31 satellite distance determinations over the past several decades, many of which employ differing distance indicators and measurement techniques (cf. McConnachie 2012). Among the most influential papers on the topic is that of Conn et al. (2012), in which probabilistic analysis techniques were applied to uniformly measure tip of the red giant branch (TRGB) distances to 27 M31 satellites using data from the PAndAS survey. These distance determinations have become central to recent studies of the M31 system, including contemporary structural parameters and the reported discovery of a thin, coherently rotating plane of satellites (Ibata et al. 2013).

However, Conn et al. (2012) emphasize that improvements to their distance determinations could be made if deeper imaging that includes the horizontal branch (HB) became available. The HB has long been known as a secure distance indicator (e.g. Vandenberg, Bolte & Stetson 1990; Carretta et al. 2000) that is more populated than the TRGB, is a well calibrated and anchored to *Hipparcos* parallaxes, and suffers from less confusion with background/foreground populations, which can lead to spurious distance determinations, particularly for galaxies with sparsely populated colour–magnitude diagrams (CMDs). We discuss prospects for improvement of the HB distnace anchor with *Gaia* in Section 4.4.

In the first paper in this series, Martin et al. (2017) presented new *Hubble Space Telescope* (*HST*) Advanced Camera for Surveys (ACS; Ford et al. 1998) imaging of 17 faint M31 satellites, that extends ∼1–2 mag below the HB. In the initial presentation of the data, Martin et al. (2017) found a preponderance of red HBs in the M31 satellites, suggestive of extended star formation histories (SFHs). Transforming this qualitative result into quantitative determinations of age requires secure distances.

In this paper, we use the sub-HB depth *HST* observations from Martin et al. (2017) to measure HB-based distances to 17 faint M31 satellites. The focus of this paper is on distance determination using the HB. Future work in this series will use these distances for a variety of M31-centric science, such as measuring SFHs.

This paper is organized as follows. In Section 2, we summarize the observations and in Section 3, we describe the distance measurement methodology. In Section 4, we present our results and compare to previous distance determinations. We provided updated distances and basic structural parameters (i.e. luminosity and half-light radius) in tabular form to facilitate use throughout the community.

2 THE DATA

Martin et al. (2017) describe the acquisition and reduction of data used in this analysis. Here, we provide a brief recap.

Using *HST*/ACS, we targeted 16 faint M31 satellites that had no previous *HST* imaging. Each galaxy was observed for a single orbit, with equal integration times split between the F606W and F814W filters. Exposures for each filter were split in half for improved cosmic ray rejection, though no dithering was performed. For each galaxy, we used DOLPHOT, a widely used point spread function stellar photometry package with modules specific to *HST* (Dolphin 2000; Williams et al. 2014), to reduce the data and construct CMDs. We ran $\sim 10^5$ artificial star tests (ASTs) per galaxy to determine the completeness and photometric errors. The 50 per cent completeness limits for these 16 systems are ∼2 mag below the HB. For a typical galaxy in the sample, the photometric uncertainties at the depth of the HB are ∼0.05 mag and the completeness is ∼80 per cent.

Beyond the initial sample of 16 systems, we added archival *HST*/ACS observations of And XVIII (HST-SNAP-13442; PI: Tully) to our sample. And XVIII was observed with the same filters and integration time as the rest of our sample. However, it is location outside the Local Group (Makarova et al. 2017) means that the 50 per cent completeness limit for And XVIII is only ∼1 mag below the HB. At the depth of its HB, the photometric uncertainties are ∼0.1 mag and the completeness is ∼65 per cent.

Martin et al. (2017) also include And XI, And XII, and And XIII data sets based on *HST* Wide Field Planetary Camera 2 (WFPC2) observations in their analysis. Owing to the different instruments and filter sets, we do not include their three systems in this distance determination paper.

Fig. 1 shows the CMDs of all 17 galaxies in our sample. The eight anchor galaxies are highlighted in orange. The *y*-axis is plotted as the pseudo-V band, which effectively flattens the HB, as described in Section 3.2. While only a minority of galaxies, i.e. the anchor sample, have a clearly discernible TRGB, nearly all galaxies have a readily identifiable HB. Martin et al. (2017) provide a detailed discussion of the stellar populations of each galaxy as revealed by its CMD.

3 METHODS

We determine the HB distances of our sample using a multistep process. First, we measure the TRGB distance to each galaxy in the native *HST* filters (i.e. F606W and F814W) using the TRGB zero-point calibration of Rizzi et al. (2007). Second, we measure the apparent magnitude of the HB in a pseudo-V band using the filter transformations provided by Rizzi et al. (2007). The purpose of this step is to 'flatten' the HB. Third, we use the set of eight galaxies that have well-defined TRGB distances to determine the mean pseudo-V band absolute magnitude for the sample. Finally, we measure the HB magnitude to all 17 galaxies and use the HB absolute magnitude calibration from the anchor sample to determine their distances. We now describe each of these steps in more detail.

3.1 Tip of the red giant branch distances

We first measure the apparent magnitude of the TRGB in all systems following the maximum-likelihood approach described in Makarov et al. (2006). We build a model power-law luminosity function (LF) with a sharp break. We convolve the LF with error distributions and completeness from the ASTs. Finally, we evaluate the likelihood function over a grid of possible TRGB magnitudes to find the maximum-likelihood value of the break. We propagate uncertainties that reflect the 68 per cent confidence interval around the maximum-likelihood value.

For 8 of the 17 systems (And IX, And XVIII, And XX, And XXIII, And XXIX, Cas III, Lac I, and Per I), we find TRGB apparent magnitudes that have finite errors, as indicated in Table 1. The remainder did not have convergent upper or lower bounds, even if a maximum-likelihood solution was found. We use these eight galaxies as our anchor sample.

We compute the distance to each of these eight systems by first correcting for Galactic foreground extinction using values

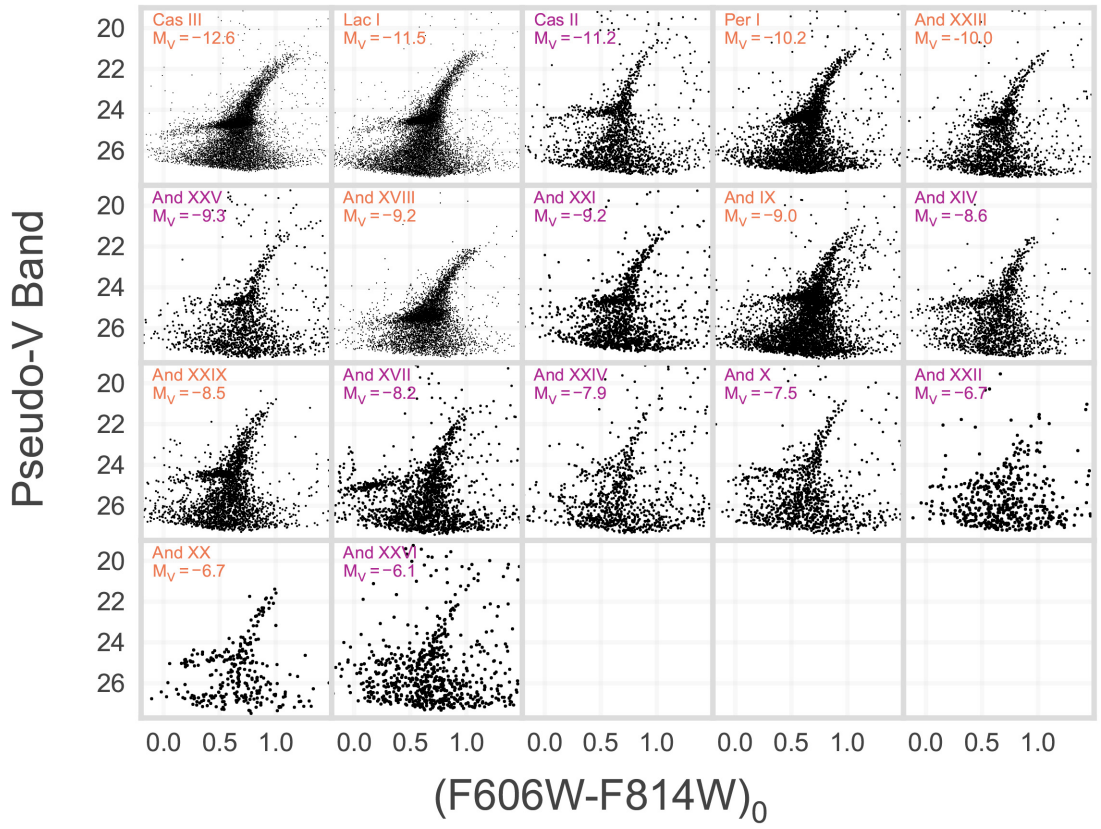

Figure 1. *HST*-based CMDs of all 17 galaxies in our sample ordered by decreasing luminosity. The CMDs are plotted as the pseudo-V band (Section 3.2), which is used to flatten the HB, versus the extinction-corrected *HST* colour. The anchor galaxies are labelled in orange. The sample covers a wide range in luminosity and stellar populations. All CMDs exhibit well-defined HBs, even if the TRGB locations are not always clear.

from Schlafly & Finkbeiner (2011). We then determine the TRGB distance to each galaxy using our extinction-corrected TRGB apparent magnitude, the extinction-corrected mean colour of the RGB, and the TRGB distance calibration in the ACS F606W and F814W filter combinations from Rizzi et al. (2007).

As a proxy for metallicity dependence, we searched for trends between TRGB magnitudes and mean RGB colour, but found no statistically significant correlations. This sample spans a narrow range in mean metallicity ($\langle$[Fe/H]$\rangle = -2.1$ to -1.7 and errors in the mean of $\sim$0.2 dex, e.g. Collins et al. 2013), thus metallicity is not expected to dramatically affect either the TRGB or HB distance determinations for our sample.

The resulting TRGB distances for all galaxies are listed in Table 1. We plot TRGB distances of the anchor sample versus their HB distances in the top panel of Fig. 2. We discuss the fidelity of the anchor sample more in Section 4.1.

3.2 Horizontal branch distances

We first measure the mean HB magnitudes for each of the eight anchor systems. To do so, we follow Rizzi et al. (2007) and transform F606W apparent magnitudes to a pseudo-V band using

$$m_{\rm V} = m_{\rm F606W_0} - 0.37\,(m_{\rm F606W_0} - m_{\rm F814W_0}) \quad (1)$$

where the above magnitudes have been corrected for extinction following Schlafly & Finkbeiner (2011). This transformation effectively 'flattens' the HB.

We then measure the mean HB magnitude for each system. We adopt a model LF of the HB that is the combination of a power law and Gaussian:

$$P(m|m_{\rm HB},\theta_0,\theta_1,\theta_2) = e^{(\theta_0\ (m-m_{\rm HB})+\theta_1)} + e^{(-0.5\ ((m-m_{\rm HB})/\theta_2)^2)} \quad (2)$$

where $\theta_{\rm i}$ are nuisance parameters, m are magnitudes from the photometry, and $m_{\rm HB}$ is the true magnitude of the HB in the pseudo-V band. Before fitting, we convolve the model with the error distribution and completeness as determined by the ASTs. The overall approach to measuring the magnitude of the HB mirrors that of our approach to measuring the TRGB. That is for each galaxy, we iterate over a grid of values for each parameter in each of the optimal values.

Because of the predominance of red HBs and the modest S/N (signal-to-noise) ratio of the data, it is not possible to easily separate the blue red clump (RC) and RGB stars from the red HB stars. Instead, we simply include the blue RC and all red HB stars in our fit. In the case of And IX, we limited HB selection to the blue HB, because of contamination from M31 halo stars. We discuss the case of And IX in Section 4.1.

As with the TRGB, we adopt the maximum-likelihood value for $m_{\rm HB}$ and uncertainties reflect the 68 per cent confidence interval around the most likely value. Note that all of the likelihood surfaces are smooth, single-valued, and reasonably narrow, such that adopting non-uniform priors on any parameter does not impact our results, i.e. our measurements are driven by the likelihood function.

Using the eight secure TRGB distances and the pseudo-V band magnitudes of the HB for the eight anchor galaxies, we

Table 1. A summary of distances measured in this paper. Galaxy names marked with an * are those in the anchor sample. Columns (2) and (3) are the *HST*-based TRGB and *HST* HB-based distance moduli from this work. Uncertainties reflect the 68 per cent confidence intervals. Values of 99.9 indicate non-convergent uncertainties. Column (4) lists ground-based TRGB distance moduli from the literature. They are all from Conn et al. (2012), except And XXIX (Bell et al. 2011), Cas III (Martin et al. 2013a), Lac I (Rhode et al. 2017), and Per I (Martin et al. 2013b). Column (5) is the *HST*-based HB linear distance to each galaxy. Column (6) is ground-based TRGB linear distance to each galaxy. Column (7) is the 3D distance of each galaxy relative to M31, assuming the *HST*-based HB distances and $\mu_{M31} = 24.47$. Column (8) is the revised absolute *V*-band magnitude. Column (9) is the revised half-light radius. Note that the *HST*-based HB and TRGB distances listed may be uncertain by up to an additional ∼40 kpc in an absolute sense due to systematic uncertainties in the TRGB zero-point. An online version of this table is available.

Galaxy name	$\mu_{TRGB,HST}$ (mag)	$\mu_{HB,HST}$ (mag)	$\mu_{TRGB,Ground}$ (mag)	$D_{HB,HST}$ (kpc)	$D_{TRGB,Ground}$ (kpc)	$D_{HB,M31}$ (kpc)	M_V (mag)	r_h (pc)
(1)	(2)	(3)	(4)	(5)	(6)	(7)	(8)	(9)
And IX*	$24.46^{+0.28}_{-0.15}$	$24.43^{+0.06}_{-0.03}$	$23.89^{+0.31}_{-0.08}$	769^{+21}_{-12}	600^{+91}_{-23}	39^{+5}_{-2}	$-9.0^{+0.3}_{-0.3}$	444^{+68}_{-53}
And X	$24.40^{+99.9}_{-99.9}$	$24.26^{+0.12}_{-0.10}$	$24.13^{+0.08}_{-0.13}$	711^{+42}_{-32}	670^{+24}_{-39}	102^{+24}_{-19}	$-7.5^{+0.3}_{-0.3}$	239^{+79}_{-39}
And XIV	$25.04^{+0.09}_{-99.9}$	$24.64^{+0.05}_{-0.04}$	$24.50^{+0.06}_{-0.56}$	847^{+21}_{-15}	793^{+23}_{-179}	178^{+11}_{-6}	$-8.6^{+0.4}_{-0.3}$	379^{+38}_{-54}
And XVII	$24.68^{+99.9}_{-99.9}$	$24.69^{+0.06}_{-0.03}$	$24.31^{+0.11}_{-0.08}$	866^{+25}_{-13}	727^{+39}_{-25}	96^{+6}_{-11}	$-8.2^{+0.3}_{-0.3}$	339^{+65}_{-51}
And XVIII*	$25.59^{+0.01}_{-0.05}$	$25.43^{+0.05}_{-0.03}$	$25.42^{+0.07}_{-0.08}$	1219^{+29}_{-13}	1214^{+40}_{-43}	458^{+12}_{-28}	$-9.2^{+0.3}_{-0.3}$	262^{+64}_{-40}
And XX*	$24.52^{+0.23}_{-0.17}$	$24.69^{+0.11}_{-0.09}$	$24.35^{+0.12}_{-0.16}$	867^{+44}_{-34}	741^{+42}_{-52}	157^{+29}_{-18}	$-6.7^{+0.5}_{-0.4}$	110^{+39}_{-29}
And XXI	$24.44^{+0.30}_{-0.23}$	$24.65^{+0.05}_{-0.03}$	$24.59^{+0.06}_{-0.07}$	851^{+19}_{-11}	827^{+23}_{-25}	145^{+11}_{-6}	$-9.2^{+0.3}_{-0.3}$	1033^{+206}_{-181}
And XXII	$24.61^{+99.9}_{-99.9}$	$24.84^{+0.27}_{-0.24}$	$24.82^{+0.07}_{-0.36}$	929^{+123}_{-99}	920^{+32}_{-129}	279^{+89}_{-49}	$-6.7^{+0.8}_{-0.5}$	253^{+86}_{-71}
And XXIII*	$24.56^{+0.18}_{-0.21}$	$24.54^{+0.06}_{-0.03}$	$24.37^{+0.09}_{-0.06}$	809^{+22}_{-10}	748^{+31}_{-21}	131^{+7}_{-2}	$-10.0^{+0.2}_{-0.3}$	1277^{+109}_{-96}
And XXIV	$24.57^{+99.9}_{-99.9}$	$24.30^{+0.28}_{-0.26}$	$24.77^{+0.07}_{-0.10}$	724^{+99}_{-81}	898^{+28}_{-42}	123^{+50}_{-30}	$-7.9^{+0.4}_{-0.4}$	579^{+208}_{-146}
And XXV	$24.52^{+99.9}_{-99.9}$	$24.60^{+0.05}_{-0.04}$	$24.33^{+0.07}_{-0.21}$	832^{+21}_{-15}	736^{+23}_{-69}	98^{+12}_{-7}	$-9.3^{+0.3}_{-0.3}$	679^{+80}_{-80}
And XXVI	$25.03^{+99.9}_{-99.9}$	$24.74^{+0.21}_{-0.20}$	$24.39^{+0.55}_{-0.53}$	887^{+89}_{-77}	754^{+218}_{-164}	150^{+43}_{-73}	$-6.1^{+0.9}_{-1.0}$	228^{+183}_{-98}
And XXIX*	$24.57^{+0.23}_{-0.22}$	$24.57^{+0.05}_{-0.04}$	$24.32^{+0.22}_{-0.22}$	820^{+17}_{-15}	973^{+32}_{-77}	195^{+4}_{-5}	$-8.5^{+0.4}_{-0.4}$	397^{+126}_{-90}
Cas II	$24.23^{+99.9}_{-99.9}$	$23.99^{+0.05}_{-0.05}$	$24.17^{+0.26}_{-0.10}$	628^{+16}_{-15}	681^{+32}_{-78}	186^{+11}_{-12}	$-11.2^{+0.4}_{-0.3}$	275^{+45}_{-40}
Cas III*	$24.57^{+0.08}_{-0.03}$	$24.70^{+0.04}_{-0.04}$	$24.45^{+0.14}_{-0.14}$	871^{+18}_{-16}	828^{+52}_{-49}	186^{+9}_{-11}	$-12.6^{+0.5}_{-0.5}$	1640^{+300}_{-240}
Lac I*	$24.51^{+0.03}_{-0.02}$	$24.50^{+0.05}_{-0.04}$	$24.40^{+0.12}_{-0.12}$	794^{+18}_{-13}	801^{+43}_{-41}	268^{+2}_{-4}	$-11.5^{+0.5}_{-0.5}$	967^{+105}_{-88}
Per I*	$24.49^{+0.14}_{-0.28}$	$24.39^{+0.05}_{-0.03}$	$24.49^{+0.18}_{-0.18}$	755^{+18}_{-9}	859^{+68}_{-63}	346^{+3}_{-1}	$-10.2^{+0.3}_{-0.3}$	384^{+98}_{-68}

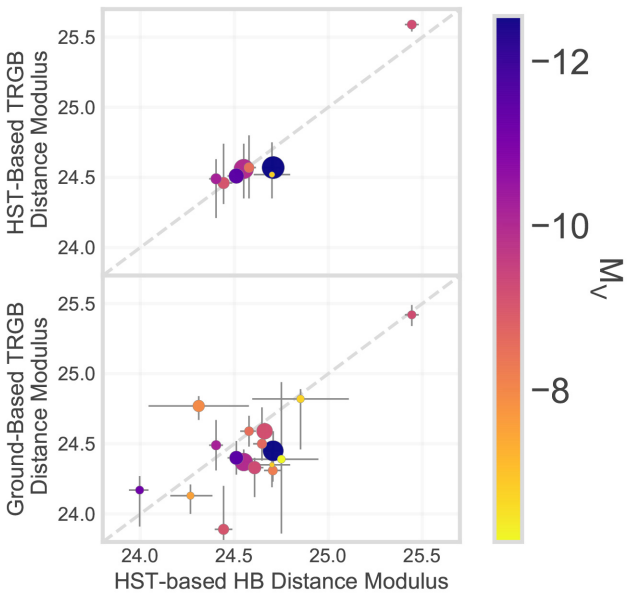

Figure 2. Top: a comparison of the *HST*-based HB and TRGB distances for the anchor sample. Points are colour-coded by luminosity and the sizes are proportional to the half-light radii. Seven of the eight galaxies are within 1σ of the mean, which is in line with statistical expectations. Bottom**:** a comparison of the *HST* HB- and ground-based TRGB distance moduli. 15 of the 17 systems have TRGB and HB distances that agree within 2σ, which is consistent with statistical expectations. The HB distances are typically ∼0.1–0.2 mag farther, and are twice as precise as the ground-based TRGB distances.

find $M(V)_{HB} = -0.43 \pm 0.03$. This value is the unweighted mean magnitude of the eight anchor galaxies distances and HB magnitudes. The uncertainty estimate includes the standard errors in the mean HB and TRGB measurements. Other averaging schemes (e.g. median, and error-weighted mean) lead to differences in the absolute magnitude at the level of $\lesssim$0.01 mag.

Following Conn et al. (2012), we do not propagate the error in the TRGB zero point (∼0.1 mag; Rizzi et al. 2007) as would be required for absolute distance determination. This is because we are primarily interested in the relative distances to the M31 satellites (e.g. to probe the structure of satellites). Thus, the distances quoted may be uncertain by an additional $\lesssim$40 kpc in an absolute sense.

Metallicity may provide another source of uncertainty in the HB calibration. The HB-based distances to Galactic globular clusters are known to be a weak function of metallicity (e.g. Carretta et al. 2000). However, this effect is likely minimal for our sample. First, as mentioned above, the mean metallicites of all galaxies in our sample span a narrow range (e.g. Collins et al. 2013). Second, because these are galaxies of mixed populations (i.e. in age/metallicity), the dependance of the HB on metallicity (or age) is diluted relative to single age/metallicity populations, i.e. Galctic globular clusters, in which the effect is more pronounced (e.g. Carretta et al. 2000).

Finally, with an HB absolute magnitude in hand for the anchor sample, we measure the HB distance to each of the remaining systems following the approach described above (i.e. pseudo-V band conversion, maximum-likelihood fitting, etc.).

4 DISTANCES TO FAINT M31 SATELLITES

Table 1 lists the *HST*-based HB and TRGB distances, ground-based TRGB distances from the literature, updated HB-based 3D distances to M31, and revised luminosities and sizes. The distance to M31 is assumed to be $\mu = 24.47 \pm 0.07$ (McConnachie et al. 2005). In this section, we briefly describe and analyse each of these topics.

4.1 Fidelity of the anchor sample

We first examine the fidelity of the anchor sample. As listed in Table 1. Each of the anchor galaxies have TRGB distance measurements with finite errors. In most cases, the TRGB uncertainties were large (∼0.1–0.2 mag) compared to the HB, which have typical measurements uncertainties of $\lesssim$0.05 mag. However, given a sample of eight systems, it is possible to define a robust mean TRGB anchor, which is all we need from the TRGB distances.

Of the eight systems, seven have absolute HB magnitudes that are within 1σ of the mean value of the anchor sample. The sole exception is And XVIII, which is consistent at the $\sim 2\sigma$ level. And XVIII is the most distant galaxy in the sample. Thus, for a fixed integration time the CMD is shallower, with the 50 per cent completeness limits extending only ∼1 mag below the HB. We examined fit residuals to the HB and TRGB of And XVIII, but did not find any obvious issues (e.g. the HB fit quality did not appear to be lower by a completeness fraction at the HB).

For the given TRGB magnitude of And XVIII, the HB would have to be 0.16 mag fainter than is observed. Conversely, the TRGB would have to be 0.16 mag brighter for the given HB magnitude. Based on the CMD of And XVIII in Fig. 1, a 0.16 mag shift of either feature is not plausible. It is at least possible that some secondary effect (e.g. chemical composition, and mass loss) is responsible for part of the discrepancy, though the data at hand are of insufficient quality for further exploration (e.g. Savino et al. 2018).

In terms of establishing the mean HB magnitude of the sample, having one of eight systems outside the 1σ range is consistent with statistical expectations.

We choose to include And IX in the anchor sample, despite some contamination from M31 halo stars, as shown in Fig. 1. The upper RGB of M31 halo stars are 0.2–0.3 mag redder than the RGB of And IX, due to the increased metallicity of M31 stars. We confirmed this by constructing the F606W–F814W CMD of the parallel WFC3/Uv-VISual (UVIS) field for And IX, which only consists of M31 halo stars. Thus, the TRGB measurement of And IX is unaffected by M31.

Given the quality of our data, the RCs and red HBs of M31 and And IX cannot be cleanly separated. Instead, we limited our HB analysis to the blue HB stars of And IX, none of which are present in the UVIS CMD of M31 stars. We find that our TRGB and HB distances to And IX are in good agreement, providing reassurance that contamination from M31 is not a large problem.

In the top panel of Fig. 2, we compare the *HST*-based HB and TRGB distances for the anchor sample. Galaxies are colour-coded by luminosity and the point sizes are proportional to their half-light radii.

As described above, seven of the eight galaxies have HB and TRGB distances that are consistent within 1σ, indicating that the process of using the TRGB anchors to calibrate the mean absolute magnitude of the HB works well. Furthermore, the average precision is generally better for our HB distances. For the most luminous galaxies in the anchor sample, both the TRGB and HB have a precision of $\lesssim$0.05 mag. However, for the fainter systems (e.g. And XX), the TRGB precision reaches ∼0.2 mag, whereas the HB precision is $\lesssim$0.05–0.1 mag.

4.2 Comparison with ground-based TRGB distances

The bottom panel of Fig. 2 compares the *HST* HB-based distances with recent TRGB distances from ground-based imaging. The majority of these measurements are from Conn et al. (2012) with TRGB distances to And XXIX, Lac I, Cas III, and Per I taken from Bell et al. (2011), Rhode et al. (2017), and Martin et al. (2013a,c), respectively. The ground-based TRGB distances are listed in Table 1.

Fig. 2 shows good general agreement between the ground-based TRGB and HB distances. Of the 17 systems, 10 (And X, And XIV, And XVIII, And XXI, And XXII, And XXVI, And XXIX, Cas II, Lac I, Per I) are all consistent within 1σ. Of the remaining systems, five galaxies (And XX, And XXIII, And XXIV, And XXV, Cas III) have TRGB and HB distances that are consistent within 2σ.

Two galaxies (And IX and And XVII) have *HST*-based HB and ground-based TRGB distances that are inconsistent at the 2σ–3σ level. The HB distances to each system place them ∼170 (And IX) and ∼140 kpc (And XVII) farther away than the TRGB distances from Conn et al. (2012).

To explore these tensions in more detail, we plot the CMDs of And IX and And XVII in Fig. 3. The orange and purple shaded bands reflect the projected 1σ location of the TRGB apparent magnitude, for the Conn et al. (2012) and our HB distances, respectively.

For both systems, the Conn et al. (2012) TRGB magnitudes appears to be a few tenths of a magnitude too bright relative to the location of the TRGB on the *HST* CMD. In comparison, the projected TRGB location from the HB-based distance seems reasonable.

As ancillary sanity checks, we compare the *HST*-based HB distances to (i) our *HST*-based TRGB distances and (ii) ground-based TRGB distances determinations from studies other than Conn et al. (2012).

In the case of And IX, we find $\mu_{\rm TRGB,HST} = 24.46^{+0.28}_{-0.15}$ mag, which compares well with $\mu_{\rm HB,HST} = 24.43^{+0.06}_{-0.05}$. Moreover, *HST*-based distances are in good agreement with the TRGB distance to And IX from McConnachie et al. (2005), of $\mu = 24.42 \pm 0.07$. From inspection of the CMD in Fig. 3, it is clear that the Conn et al. (2012) distance of $\mu = 23.89^{+0.31}_{-0.08}$ is not compatible with the TRGB location of And IX. Given And IX's projected proximity to M31, it is possible that contamination from M31 affected the Conn et al. (2012) measurement.

For And XVII, we find a best-fitting *HST*-based TRGB distance of $\mu_{\rm TRGB,HST} = 24.68$, which is identical to the best-fitting HB distance. The TRGB fitting routine does not converge on finite uncertainties due to the sparsity of the TRGB. The TRGB distance from discovery paper of And XVII is $\mu = 24.50 \pm 0.1$ (Irwin et al. 2008). This effectively splits the difference between our distance determination and that of Conn et al. (2012). Inspection of the CMD of And XVII in Fig. 3 shows that the Conn et al. (2012) distance of $\mu = 24.31^{+0.11}_{-0.08}$ produces too bright of a TRGB location. One challenge in determining the TRGB distance to And XVII is that the TRGB is sparsely populated in both the *HST*- and ground-based data.

Recently, Martínez-Vázquez et al. (2017) used deep, high-cadence *HST* imaging to measure RR Lyrae-based distances to six M31 satellites (And I, And II, And III, And XV, And XVI,

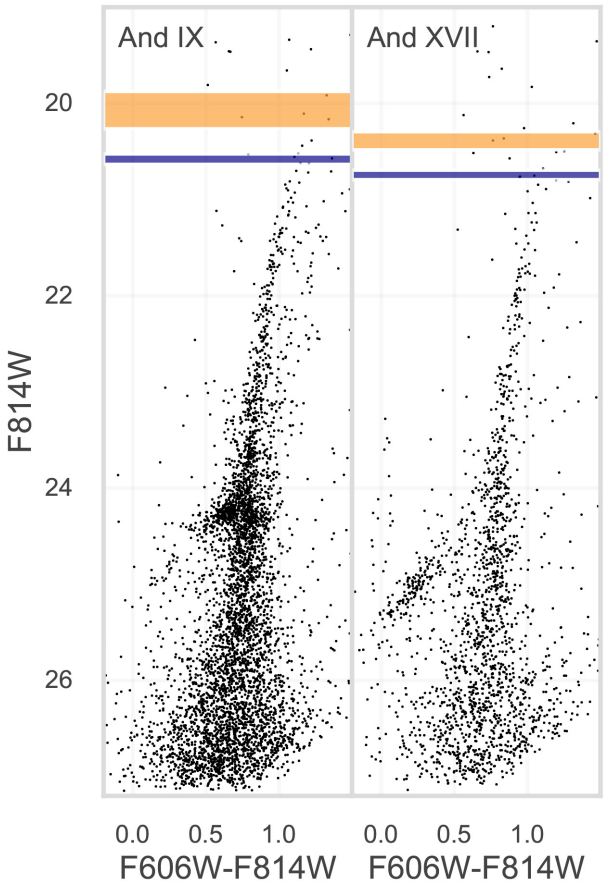

Figure 3. CMDs for the two systems (And IX and And XVII) for which the ground-based TRGB and *HST*-based HB distances are in disagreement. The orange band indicates the 1σ range for the TRGB magnitude inferred from the ground-based TRGB distance. The purple band is the same, but using our HB distance. In both cases, the ground-based TRGB distance appears to be too bright. This may be the result of contamination from MW foreground stars confusing the TRGB fitting algorithm.

And XXVIII). Unfortunately, this sample does not overlap with ours, prohibiting a direct comparison. However, because the two samples are anchored to the same zero-point (Carretta et al. 2000; Rizzi et al. 2007), it is instructive to compare the RR Lyrae distances to the TRGB distances of Conn et al. (2012).

For the five galaxies that Martínez-Vázquez et al. (2017) and Conn et al. (2012) have in common (And XXVIII is not included in the Conn et al. 2012 sample), only And III is consistent within 1σ. Otherwise, the distances reported by Martínez-Vázquez et al. (2017) are ∼0.2–0.4 mag more distant than the Conn et al. (2012) TRGB distances. Our HB distances are also slightly larger than the Conn et al. (2012) values. A detailed comparison of these two distance sets (ground-based TRGB and *HST*-based RR Lyrae) is beyond the scope of this paper. For consistency with HB-distances from the present work, we recommend adopting those of Martínez-Vázquez et al. (2017).

Overall, there is general good agreement between the new HB and previous TRGB distances. As a result, the structural properties of the faint M31 satellites do not change much. However, for completeness, we use our *HST*-based HB distances and the structural measurement code described in Martin et al. (2016) to update the half-light radii and luminosities of the 17 faint galaxies in our sample. The results are listed in Table 1.

The general good agreement in our HB and the Conn et al. (2012) TRGB distances mean that the broad configuration of the faint M31 satellites (e.g. with respect to the plane; Ibata et al. 2013) remains nearly the same.

4.3 Distance precision

One result of this work is an improved precision in the distances of faint M31 satellites. Across the sample, the ground-based TRGB relative distances are precise to ∼7 per cent (e.g. Conn et al. 2012). In contrast, the *HST*-based TRGB distances are less precise. *HST* covers a smaller area of each galaxy. As a result the *HST*-based CMDs have fewer TRGB stars, which makes it more challenging to clearly define the location of the TRGB.

In comparison, the *HST*-based HB distances have a typical precision of ∼4 per cent (Table 1). At a distance of 800 kpc, the precision in distance moduli translate to a linear distance precision of ∼56 kpc (7 per cent) and ∼35 kpc (4 per cent), respectively. The improve precision provided by *HST* is largely due to the better definition of the HB than the TRGB for the faintest systems, along with reduced contamination, as the Milky Way (MW) foreground does not pollute the HB region of the CMD as much as it does the TRGB at the distance of M31. As discussed below, similar or better precision may be achievable with ground-based imaging that includes the HB.

In two cases (And XXII, and And XXIV), the distance precision on the HB is worse than the ground-based TRGB. For And XXII, the *HST*-based CMD is so sparsely populated that the HB and TRGB are challenging to define, which leads to larger uncertainties. Because *HST* covers $\sim 2\,r_{\rm h}$, wider area imaging would like result in modest gains in precision, due to the declining stellar density as a function of radius. These two systems illustrate challenges in distance determinations for faint systems at large distances: the HB is usually a more precise distance indicator than the TRGB, but only when its mean magnitude can be accurately measured.

In principle, the ability to measure precise HB distances of faint galaxies at the distance of M31 is not a unique capability of *HST*. With sufficient integration time, a large ground-based telescope (e.g. Subaru/Hyper Suprime-Camera, and the Large Synoptic Survey Telescope) can produce CMDs that include the HB. In some cases, the larger areal coverage would improve the HB distance precision because more stars would be included. In other cases, e.g. systems in which *HST* areal coverage includes 1–2 half-light radii, the increased areal coverage will have diminishing return. For galaxies with higher surface brightness, crowding from the ground may be an issue. Alternatively, measuring even a handful of RR Lyrae may be a better way of measuring distances to faint systems with ill-defined HBs and/or TRGBs (e.g. Sesar et al. 2014; Martínez-Vázquez et al. 2017).

4.4 Future prospects

Perhaps the most critical future application of HB distances will be for ultrafaint dwarf galaxies (UFD) discovered in the field ($D \gtrsim 300$ kpc). In such systems, the TRGB will almost certainly be poorly populated, compromising its utility as a distance indicator.

Predictions suggest that hundreds, or more, UFDs may exist within a few Mpc (e.g. Garrison-Kimmel et al. 2014). Deep wide-area surveys such as LSST should shepherd in a new era of discovery at large distances (e.g. Ivezić et al. 2019). As more faint galaxies are discovered in the field, it remains imperative that we obtain precise and accurate distances, which are fundamental to the rich

science that is uniquely possible with resolved faint galaxies (e.g. Bullock & Boylan-Kolchin 2017; Simon 2019).

Though the HB can provide precise distances to faint systems, it does have drawbacks. One is its faintness. The HB is ∼4 mag dimmer than the TRGB in optical bands. Thus, more integration time is required to observe the HB at a fixed S/N.

A second drawback is its wavelength sensitivity. Though the HB is an ideal distance indicator at mid-optical wavelength (e.g. *V* band), it is not as useful in the near-IR. For increasingly red bandpasses, the HB is no longer horizontal; the blue HB becomes much fainter than the red HB. Thus, for galaxies that are expected to have prominent blue HBs, e.g. ancient metal-poor galaxies, near-IR, and redder, observations of the HB will not be as useful as optical observations.

A third challenge is crowding. Optical surveys such as Dark Energy Survey and LSST have the potential to provide very precise HB-based distances throughout the LG. However, beyond the LG, crowding may be more of a challenge, and the angular resolution afforded by space (e.g. *Euclid*, *the James Webb Space Telescope*, and *Wide-Field Infrared Survey Telescope*) or adaptive optics (e.g. the Giant Magellan Telescope, the Thirty Mmeter Telescope) may be required to reach the HB.

However, many of these facilities are near-IR optimized, which are is useful for HB distance determinations, as discussed above. Thus, as UFDs are discovered in the field, it may be beneficial to prioritize *HST* observations of them in order to measure reliable HB distances. As demonstrated in this work, even at distances of ∼1 Mpc, only 1–2 orbits per galaxy would be to measure precise HB distances for galaxies brighter than $M_V \sim -6$.

Though this paper focused on relative distances, it is scientifically useful to measure absolute distances from the HB (e.g. for UFDs). Determining absolute distances to high precision requires improving anchor of the HB distance scale. Carretta et al. (2000) provide an excellent overview of how the HB distance scale is anchored. To briefly summarize: the HB distance scale is currently based on *Hipparcos* parallaxes to ∼20 metal-poor subdwarfs located in the field. The properties of these subdwarfs (e.g. luminosity, colour, and metallicity) were used to re-derive new distances to metal-poor Galactic globular clusters. Based on these revised globular cluster distances and photometry of their HBs, Carretta et al. (2000) provide a relationship between absolute *V*-band magnitude of the HB and metallicity. The widely used TRGB distance calibrations of Rizzi et al. (2007) are also anchored to this scale.

Gaia (Gaia Collaboration et al. 2016) presents a clear opportunity to improve the anchor of the HB (and TRGB) absolute distance scale. For HB stars, most direct approach would be to measure parallaxes of metal-poor Galactic HB stars, either in the field or in GCs. This approach is similar to HB distance studies conducted with *Hipparcos* (e.g. Koen & Laney 1998; Gratton 1998; Popowski & Gould 1998).

However, Gaia Collaboration et al. (2018) show that few metal-poor HB stars (though more than *Hipparcos*) and no GCs have sufficiently accurate parallaxes to serve as a direct anchor. This situation could improve as the *Gaia* mission continues and parallaxes with small errors become available to larger distances.

An alternative approach is to use the metal-poor subdwarf fitting approach outlined in Carretta et al. (2000) to revisit and/or improve their HB distance calibration. *Gaia* provides for an expanded sample of metal-poor subdwarfs with precise parallaxes. A larger sample would both improve the random uncertainties and help to better quantify systematic uncertainties, which can be challenging to do from small samples. In addition, stellar spectra from *Gaia*, and other Galactic stellar spectroscopy surveys (e.g. Cui et al. 2012; De Silva et al. 2015; Majewski et al. 2017), now provide for improved abundance and metallicity determinations. These can be used to, for example, better determine the chemical patterns in the subdwarfs as well as for HB stars in the globular clusters.

To the best of our knowledge, *Gaia* distances to metal-poor subdwarfs have primarily been used to test stellar evolution models (e.g. O'Malley, Gilligan & Chaboyer 2017), but not re-evaluate the HB distance scale. Thus, there appears to be ample opportunity for *Gaia* to make an impact in this area, and ultimately improve the entire Population II distance ladder.

ACKNOWLEDGEMENTS

Support for HST program GO-13699 was provided by NASA through a grant from the Space Telescope Science Institute, which is operated by the Association of Universities for Research in Astronomy, Incorporated, under NASA contract NAS5-26555. These observations are associated with program HST-SNAP-13442 and HST-GO-13699. DRW acknowledges support from an Alfred P. Sloan Fellowship and an Alexander von Humboldt Fellowship. SMA is supported by the National Science Foundation Graduate Research Fellowship under Grant DGE 1752814. This research has made use of the NASA/IPAC Extragalactic Database (NED) which is operated by the Jet Propulsion Laboratory, California Institute of Technology, under contract with the National Aeronautics and Space Administration. This research made use of Astropy,[1] a community-developed core PYTHON package for Astronomy (Astropy Collaboration et al. 2013, 2018).

REFERENCES

Abazajian K. et al., 2003, AJ, 126, 2081
Astropy Collaboration et al., 2013, A&A, 558, A33
Astropy Collaboration et al., 2018, AJ, 156, 123
Bell E. F., Slater C. T., Martin N. F., 2011, ApJ, 742, L15
Bullock J. S., Boylan-Kolchin M., 2017, ARA&A, 55, 343
Carretta E., Gratton R. G., Clementini G., Fusi Pecci F., 2000, ApJ, 533, 215
Chambers K. C. et al., 2016, preprint(arXiv:1612.05560)
Collins M. L. M. et al., 2013, ApJ, 768, 172
Conn A. R. et al., 2012, ApJ, 758, 11
Cui X.-Q. et al., 2012, Res. Astron. Astrophys., 12, 1197
De Silva G. M. et al., 2015, MNRAS, 449, 2604
Dolphin A. E., 2000, PASP, 112, 1383
Ford H. C. et al., 1998, in Bely P. Y., Breckinridge J. B., eds, Proc. SPIE Conf. Ser. Vol. 3356, Space Telescopes and Instruments V. SPIE, Bellingham, p. 234
Gaia Collaboration et al., 2016, A&A, 595, A1
Gaia Collaboration et al., 2018, A&A, 616, A10
Garrison-Kimmel S., Boylan-Kolchin M., Bullock J. S., Lee K., 2014, MNRAS, 438, 2578
Gratton R. G., 1998, MNRAS, 296, 739
Ho N., Geha M., Tollerud E. J., Zinn R., Guhathakurta P., Vargas L. C., 2015, ApJ, 798, 77
Ibata R., Martin N. F., Irwin M., Chapman S., Ferguson A. M. N., Lewis G. F., McConnachie A. W., 2007, ApJ, 671, 1591
Ibata R. A. et al., 2013, Nature, 493, 62
Irwin M. J., Ferguson A. M. N., Huxor A. P., Tanvir N. R., Ibata R. A., Lewis G. F., 2008, ApJ, 676, L17
Ivezić, Ž. et al., 2019, ApJ, 873, 111
Kalirai J. S. et al., 2010, ApJ, 711, 671

[1] http://www.astropy.org

Koen C., Laney D., 1998, MNRAS, 301, 582
Majewski S. R. et al., 2017, AJ, 154, 94
Makarov D., Makarova L., Rizzi L., Tully R. B., Dolphin A. E., Sakai S., Shaya E. J., 2006, AJ, 132, 2729
Makarova L. N., Makarov D. I., Karachentsev I. D., Tully R. B., Rizzi L., 2017, MNRAS, 464, 2281
Martínez-Vázquez C. E. et al., 2017, ApJ, 850, 137
Martin N. F. et al., 2009, ApJ, 705, 758
Martin N. F. et al., 2013a, ApJ, 772, 15
Martin N. F. et al., 2013c, ApJ, 779, L10
Martin N. F. et al., 2016, MNRAS, 458, L59
Martin, N. F. et al., 2017, ApJ, 850, 15
Martin N. F., Ibata R. A., Irwin M. J., Chapman S., Lewis G. F., Ferguson A. M. N., Tanvir N., McConnachie A. W., 2006, MNRAS, 371, 1983
Martin N. F., Ibata R. A., McConnachie A. W., Dougal Mackey A., Ferguson A. M. N., Irwin M. J., Lewis G. F., Fardal M. A., 2013b, ApJ, 776, 80
McConnachie A. W. et al., 2008, ApJ, 688, 1009
McConnachie A. W. et al., 2018, ApJ, 868, 55
McConnachie A. W., 2012, AJ, 144, 4
McConnachie A. W., Irwin M. J., 2006, MNRAS, 365, 1263
McConnachie A. W., Irwin M. J., Ferguson A. M. N., Ibata R. A., Lewis G. F., Tanvir N., 2005, MNRAS, 356, 979
O'Malley E. M., Gilligan C., Chaboyer B., 2017, ApJ, 838, 162
Popowski P., Gould A., 1998, ApJ, 506, 271
Rhode K. L., Crnojević D., Sand D. J., Janowiecki S., Young M. D., Spekkens K., 2017, ApJ, 836, 137
Richardson J. C. et al., 2011, ApJ, 732, 76
Rizzi L., Tully R. B., Makarov D., Makarova L., Dolphin A. E., Sakai S., Shaya E. J., 2007, ApJ, 661, 815
Savino A., de Boer T. J. L., Salaris M., Tolstoy E., 2018, MNRAS, 480, 1587
Schlafly E. F., Finkbeiner D. P., 2011, ApJ, 737, 103
Sesar B. et al., 2014, ApJ, 793, 135
Simon J. D., 2019, preprint(arXiv:1901.05465)
Slater C. T., Bell E. F., Martin N. F., 2011, ApJ, 742, L14
Tollerud E. J. et al., 2012, ApJ, 752, 45
Vandenberg D. A., Bolte M., Stetson P. B., 1990, AJ, 100, 445
Vargas L. C., Geha M. C., Tollerud E. J., 2014, ApJ, 790, 73
Williams B. F. et al., 2014, ApJS, 215, 9
Zucker D. B. et al., 2004, ApJ, 612, L121
Zucker D. B. et al., 2007, ApJ, 659, L21

SUPPORTING INFORMATION

Supplementary data are available at *MNRAS* online.

m31_table1.dat

Please note: Oxford University Press is not responsible for the content or functionality of any supporting materials supplied by the authors. Any queries (other than missing material) should be directed to the corresponding author for the article.

This paper has been typeset from a TEX/LATEX file prepared by the author.